CRYSTAL GROWTH & DESIGN
2008
VOL. 8, NO. 6
1785–1788

Communications

Optical Emissions of Zn and ZnO in Zn-ZnO Structure Synthesized by Electrodeposition with Aqueous Solution of Zinc Nitrate-6-hydrate

Ming-Kwei Lee* and Hwai-Fu Tu

Department of Electrical Engineering, National Sun Yat-sen University, Kaohsiung, 80424, Taiwan, R. O. C.

Received November 29, 2006; Revised Manuscript Received February 17, 2008

ABSTRACT: Both hexagonal zinc and wurtzite zinc oxide were deposited on p-type silicon substrate by the electrodeposition with an aqueous solution of zinc nitrate-6-hydrate near room temperature. Zinc dominates the growth at higher current density, and zinc oxide dominates the growth at higher deposition temperature. The optical emission from zinc and zinc oxide nanostructures are observed from microphotoluminescence spectra.

Zinc oxide (ZnO) with wide direct band gap of 3.37 eV and high excitonic binding energy of 60 mV is a promising material for optoelectronic applications. It can perform ultraviolet (UV) emission at room temperature (RT).[1] Several reports indicate that ZnO has high photocatalytic efficiency.[2–4] The semiconductor-metal nanocomposites are expected to have higher potentials in catalysis, optics, and magnetic applications.[5–7] Recently, Zn-ZnO nanocomposites was obtained using $ZnCl_2$ electrolyte by the electrodeposition method at room temperature.[8] The electrodeposition method is an efficient way to prepare ZnO films at low temperature.[2] The shape and size of ZnO can be modulated by the cathodic potential, current density,[2] or adding molecular agents into the electrolyte.[3] On the other hand, the electrolyte of zinc nitrate-6-hydrate electrolyte used for Zn-ZnO nanocomposites formation can prevent Cl_2 contamination and meets the requirement of environmental protection. However, only ZnO was obtained at various deposition temperatures,[9] which could result from the lower applied current density. In this paper, a higher current density was used to prepare Zn-ZnO nanocomposites using zinc nitrate-6-hydrate electrolyte. The formation mechanism of Zn-ZnO nanocomposite and the role of Zn were also investigated.

Several papers have been reported to prepare electrodeposited ZnO films at temperatures above 60 °C on conductive electrodes, for example, indium tin oxide,[2,4] fluorine-doped tin oxide,[10] or n-type silicon[4] and gallium nitride[11] substrates. Boron-doped P-type (100) Si wafer with resistivity of 1−10 Ω-cm was used as the substrate in this experiment. The p-Si wafer is rarely used in electrodeposition, and we developed a simple way to deposit ZnO onto it. By this method, we can further build a structure of high quality n-ZnO on p-substrates to apply p-n junction devices. Otherwise, the heterojunction of n-ZnO and p-Si has the potential to separate the electron and hole and benefits the photocatalysis.

* To whom correspondence should be addressed. Tel: 886-7-5252000 ext. 4120; fax: 886-7-5254199; e-mail: mklee@mail.ee.nsysu.edu.tw.

Aluminum cathode was evaporated on the backside of the Si substrate. It was then coated with photoresist for the protection of the Al electrode during ZnO growth. A platinum sheet was used as the anode electrode. 0.1 M zinc nitrate-6-hydrate aqueous solution was used as the electrolyte. In order to investigate the function of current density (fixed at 0.1, 1, 10, and 20 mA/cm^2) for electrodepsited ZnO, the deposition temperature was fixed at 30 °C. In order to investigate the function of deposition temperature (fixed at 30 and 65 °C), the current density was fixed at 20 mA/cm^2. The total deposition time was 20 min. The relationship between the current density and the electric charge is described as $J = q/At$, where J is the current density, A is the area, q is the electric charge (Coulomb), and t is the time. The A and t are fixed in this study, so the electric charge increases with the current density. By the equation, the electric charges for applied current densities of 0.1, 1, 10, and 20 mA/cm^2 are 0.12, 1.2, 12, 24 C/cm^2. The thicknesses for applied current densities of 0.1, 1, 10, and 20 mA/cm^2 are about 0.5, 0.8, 3, and 8 μm for the deposition of 20 min.

These conditions are comparable to the standard deposition on a metal electrode (ITO).[12] The thicknesses for applied current densities of 0.1, 1, 10, and 20 mA/cm^2 are about 0.5, 0.8, 3, and 8 μm for the deposition of 20 min. P-Si substrate is etched in dilute HF solution to remove natural SiO_2 before electrodeposition. SiO_2 will be formed more or less after P-Si substrate is immersed in electrolyte. Moreover, OH^- ions in electrolyte for SiO_2 formation are repelled by the applied negative potential on P-Si substrate. The Schottky interface is formed between p-type Si and electrolyte. The sufficient high positive potential across the Schottky interface will induce the band bending of p-Si conduction band and reach the inversion state. The electrons in electrolyte can transport via the n-type inversion state on the p-type wafer surface. The deposition potentials are 2.8, 4.2, 10.9, 16.2 V for 0.1, 1, 10, and 20 mA/cm^2 in the present case. The deposition potential is 16.2 V for 20 mA/cm^2, which is a large cathodic potential. It is suitable

10.1021/cg060857t CCC: $40.75
Published on Web 04/23/2008

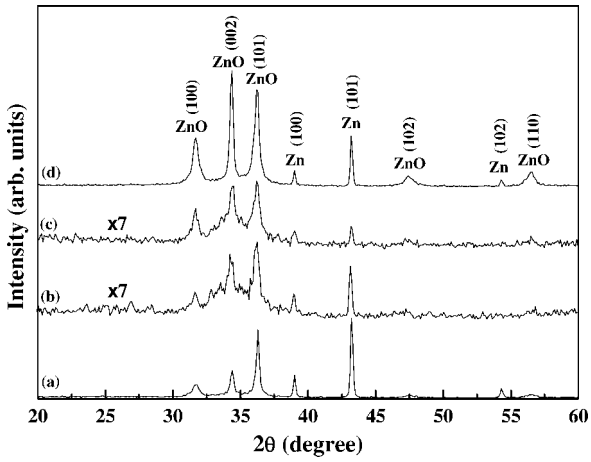

Figure 1. XRD analyses of electrodeposited Zn-ZnO prepared at different current densities (a) 20, (b) 10, (c) 1 mA/cm^2 at 30 °C, and (d) 20 mA/cm^2 at 65 °C.

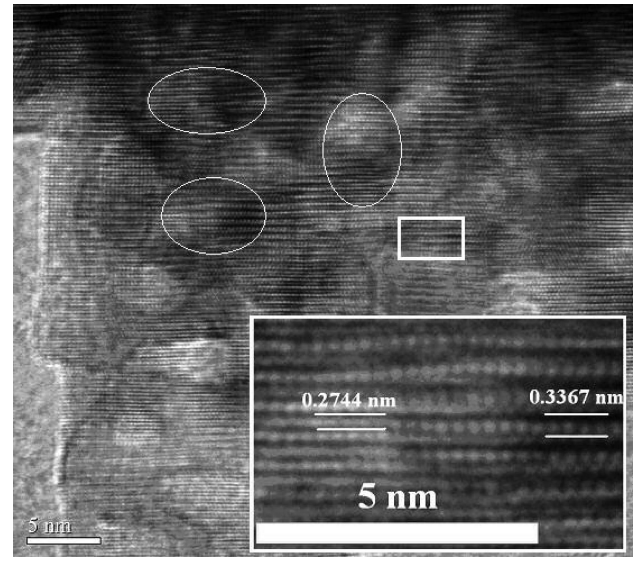

Figure 2. TEM image of Zn-ZnO nanostructure prepared at 30 °C with the applied current density of 20 mA/cm^2.

for the deposition of higher Zn/ZnO ratio and investigates the optical emission of Zn. We did not observe any negative effects.

The crystallinity was examined by X-ray diffraction (XRD). The chemical composition of the deposited films was examined by the energy dispersed X-ray (EDX) analysis. The structure is observed by field emission scanning electron microscope (FE-SEM) (XL-40FEG). The micro photoluminescence (micro-PL) was used to characterize the optical properties at room temperature. Fourier transform infrared (FTIR) spectroscopy was used to examine the chemical bonds with a resolution of 2 cm^{-1}.

The mechanisms for Zn-ZnO growth by the electrodeposition method are proposed as follows.

$$Zn^{2+} + 2e \rightarrow Zn \quad (1)$$

$$Zn^{2+} + 2OH^- \rightarrow Zn(OH)_2 \, (\Delta H > 0) \quad (2)$$

$$Zn(OH)_2 \rightarrow ZnO + H_2O \, (\Delta H > 0) \quad (3)$$

Zn^{2+} ions in the electrolyte will form Zn on Si cathode via eq 1, or react with hydroxide ions to form zinc hydroxide ($Zn(OH)_2$) via eq 2 and then dehydrate into ZnO via eq 3 depending on the current density and the deposition temperature.[13]

Figure 1 shows the XRD spectra of deposited films prepared at different current densities of (a) 20, (b) 10, (c) 1 mA/cm^2 at 30 °C, and (d) 20 mA/cm^2 at 65 °C. For the current density of 0.1 mA/cm^2, only very thin ZnO with very weak XRD spectrum is obtained due to too low growth rate. The hexagonal Zn peaks increase with increasing the current density as shown in Figure 1a−c. Although the EDX cannot give an accurate quantitative analysis for thin films, especially oxide films, it can give a good reference. The atomic ratios of Zn/O also increase with an increase in the current density analyzed by EDX. From previous reports,[2–4,8,10,11] Zn was not observed (60−80 °C), which could result from the lower deposition current by electrodeposition method. Zn deposition and the reaction with hydroxide ions compete in the whole process. The transporting velocity of electroactive species is proportional to the current density. It can be described as $v = j/nF$, where v is the velocity, j the current density, n the number of electrons, F the Faraday constant. High current density will increase the velocity of Zn^{2+} and more Zn can be reduced on Si substrate. The reaction rate of Zn ions with hydroxide ions is higher than the Zn deposition rate for low current density. Higher deposition temperature will drive eqs 2 and 3 toward the right due to the endothermic reactions. Therefore, Zn decreases and ZnO increases in the films examined by the XRD spectrum shown in Figure 1d, in which the deposition temperature is 65 °C. It can be further confirmed by TEM analysis. Figure 2 shows the high resolution transmission electron microscope (HR-TEM) image of electrodeposited Zn-ZnO nanostructure prepared at the current density of 20 mA/cm^2 at 30 °C. As shown in the inset, the spaces are 0.2744 and 0.3367 nm in accordance with the lattice constants of Zn and ZnO (JCPDS files, $a = 0.2665$ nm for Zn and 0.3298 nm for ZnO). It confirms that the nanostructure containing Zn-ZnO. ZnO are randomly distributed in the Zn-ZnO structure. Some regions containing both Zn-ZnO are marked by white circles. The Zn nanoparticle is formed from eq 1. The Zn undergoes a reaction with OH ions and dehydration process to form ZnO as eqs 2 and 3. The size of Zn nanoparticles was determined by the factor of applied current density which corresponds to the overpotential.[14] It is consistent with the analyses by XRD. The grain sizes of ZnO are calculated by Scherrer's equation, $t = 0.9\lambda/B \cos \theta_B$, where t is the grain size, λ is the wavelength of X-ray, B is the full width at half-maximum (fwhm) in radians of the peak, θ_B is the degree of diffraction peak. The grain sizes of ZnO prepared at different current densities of 1, 10, and 20 mA/cm^2 at 30 °C and 20 mA/cm^2 at 65 °C are about 23, 26, 37, and 44 nm. The grain size of ZnO increases with the applied current density and the deposition temperature.

The PL spectrum was not observed for the film prepared at the current density of 0.1 mA/cm^2 at 30 °C. It could be from the very thin ZnO film. Figure 3 shows the PL spectra of Zn-ZnO prepared at (a) 20, (b) 10, and (c) 1 mA/cm^2 current density at 30 °C, and (d) 20 mA/cm^2 at 65 °C excited with He-Cd 325 nm laser. The intensity ratios of the ultraviolet-light to visible light for Zn-ZnO prepared at different current densities 1, 10, and 20 mA/cm^2 at 30 °C and 20 mA/ cm^2 at 65 °C are 3.5, 5.6, 104, and 5.0. The quality of ZnO is higher with an increase in the applied current density and a decrease in the deposition temperature. All PL spectra show a weak peak at 344 nm, which is independent of the preparation conditions as shown in the inset of Figure 3. The PL intensity at 344 nm increases with a decrease in the current density but an increase in the deposition temperature. Therefore, the peak ought to be from the energy transition of zinc nanoparticles similar to the report of a recent paper.[15]

The PL peak intensity at 374 nm from ZnO increases with an increase in the deposition current density and a decrease in the deposition temperature. It comes from the fact that the total ZnO volume increases with an increase in the deposition current density and a decrease in the deposition temperature. At the same time, the ZnO volume increases with a decrease in the Zn volume in a Zn-ZnO nanoparticle. That is to say, the Zn/ZnO ratio increases with an increase in the deposition current density and a decrease in the deposition temperature. Therefore, the PL peak intensity at

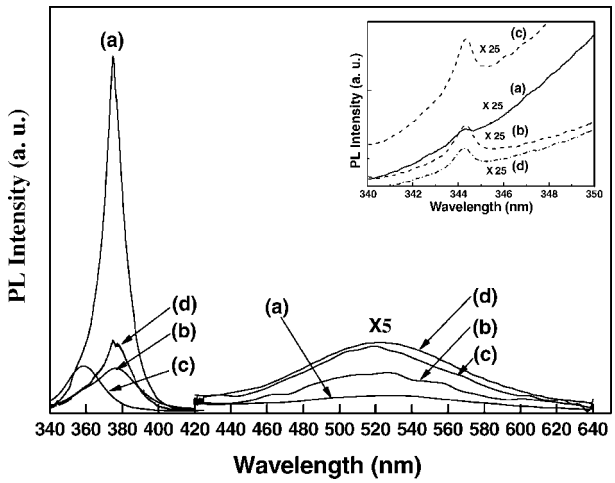

Figure 3. Micro-PL analyses of electrodeposited Zn-ZnO prepared at different current densities (a) 20, (b) 10, (c) 1 mA/cm^2 at 30 °C, and (d) 20 mA/cm^2 at 65 °C.

374 nm associated ZnO shows an opposite trend with the intensity of the Zn PL peak. The PL peaks at 374 and 380 nm are from ZnO bound excitons related to oxygen vacancies and interstitial zinc[16] as shown in Figure 3d because the concentrations of these defects increase with the deposition rate at a higher temperature. It is consistent with the XRD observation. The strong PL ultraviolet light is from the high-quality ZnO prepared by the electrodeposition method. It is supported by the strong XRD peaks shown Figure 1, and the regular lattice arrangement shown in Figure 2.

Compared with Cao and Li et al. report, they conjectured that the UV light is associated with the quality of electrodeposition ZnO. Their ZnO with less defects is transformed from $Zn(OH)_2$. The stoichiometric $Zn(OH)_2$ is obtained by the sufficient reaction with OH^- at higher deposition temperature of 60 °C with a lower deposition rate. So the intensity of UV light is strong.[17–19] Izaki et al. reported that high-quality ZnO is deposited with Au buffer layer under almost similar deposition conditions with the report by Cao and Li et al., but a weak UV emission is obtained. The wavelength of UV and visible emissions is affected by cathodic potential, which suggests that the ZnO quality is influenced by impurity and hydroxide.[20] In our paper, the high quality and stronger UV intensity ZnO is transformed from the oxidation of Zn directly with OH^-. High Zn/ZnO ratio is obtained from the insufficient reaction with OH^- at lower deposition temperature and higher deposition current density.

Figure 4a−c show the SEM images of applied current densities at 20, 10, and 1 mA/cm^2, respectively. The morphology varies with the current density. While the current density increases to 20 mA/cm^2, nanospheres are observed in Figure 4. The nanospheres are aggregates of granular Zn and ZnO grains examined by TEM shown in Figure 2. Figure 4b shows a large number of elongated and entangled nanowires. The average of these nanowires is about 70 nm in width from the inset. In Figure 4c, upper and lower images show the top and cross-sectional views of Zn-ZnO nanostructures on Si substrate. From the top view, both lying nanowires with longer length and standing nanorods with short length exist on Si surface. The standing nanorods are shown clearly in the lower image. The average radius of Zn-ZnO nanorods shown in Figure 4c is about 10 nm. The radius of ZnO nanostructures in the Zn-ZnO structures should be less than 10 nm due to Zn nanostructures were intervened in the Zn-ZnO structure which relatively leads to the size reduction of ZnO. So, its photoluminescence peak at 360 nm for Zn-ZnO nanostructure fabricated at the current density of 1 mA/cm^2 at 30 °C could result from the quantum size effect of ZnO nanostructures.[21] It is similar to the postannealed electrodeposited ZnO nanostructures, which shows the wavelength shift of UV emission in different nanostructures.[3]

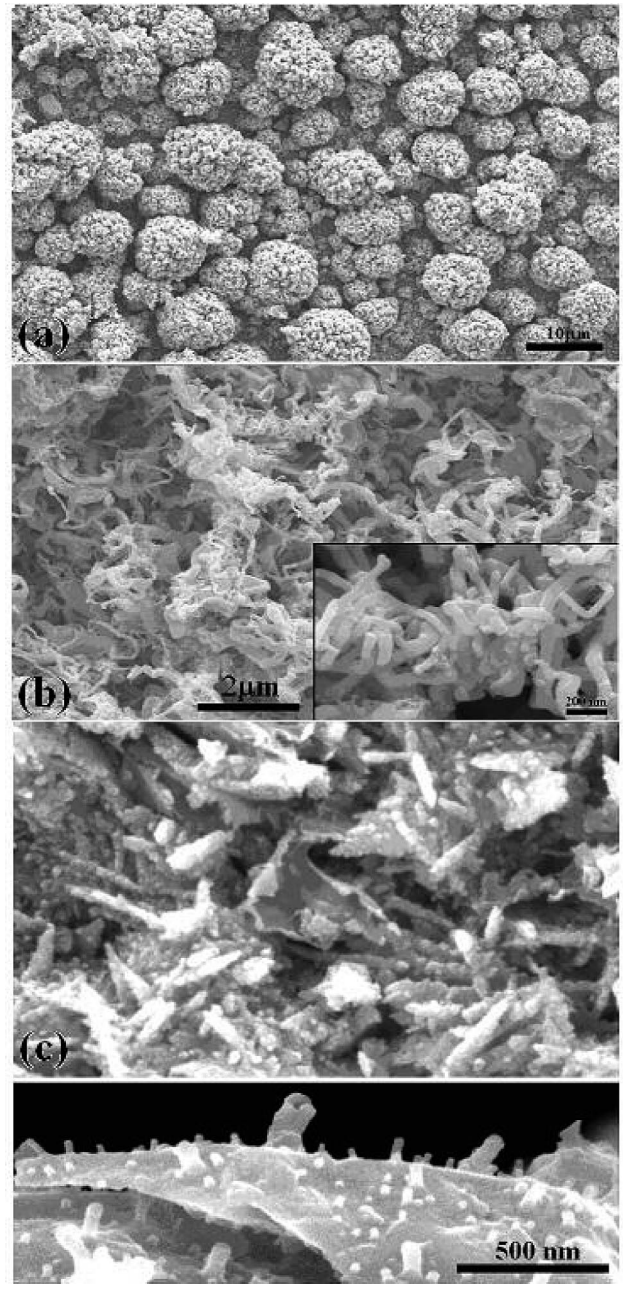

Figure 4. SEM images of Zn-ZnO nanostructures fabricated by adjusting the applied current densities (a) 20 mA/cm^2, (b) 10 mA/cm^2, and (c) 1 mA/cm^2 at 30 °C.

A broadband centered at 525 nm is associated with ZnO intrinsic defects.[22] The mechanism is examined by FTIR as follows. FTIR spectra shown in Figure 5 are samples prepared with (a) 20, (b) 10, and (c) 1 mA/cm^2 at 30 °C, and (d) 20 mA/cm^2 at 65 °C. The broadband centered at 3450 cm^{-1} is assigned to OH in Zn-ZnO. It decreases with the current density and increases with the deposition temperature. It could be from the reaction of OH^- with the interface of Zn/ZnO to form interface defects.[23] The electrons were excited from valence band to conduction band of ZnO and trapped by the interface defects and back to valence band of ZnO with a radiative path.[24] The interface defects will lower the PL UV emission and enhance the PL broad green band. Therefore, the intensity of broad green emission band centered at 525 nm increases with decreasing the current density and increasing the deposition temperature. It has the opposite trend with that of the peak at 374 nm.

In summary, the structures of hexagonal Zn and wurtzite ZnO are obtained by an electrodeposition method with an aqueous

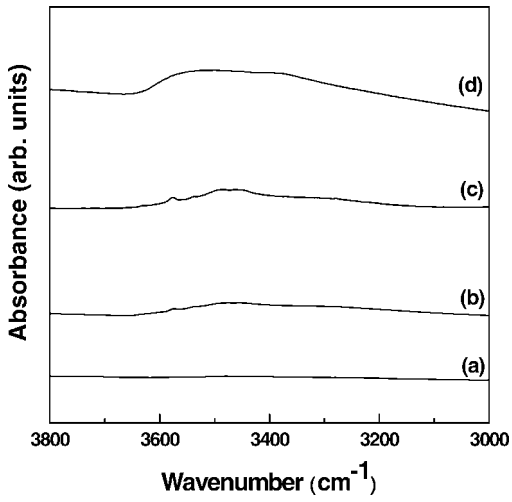

Figure 5. FTIR analyses of electrodeposited Zn-ZnO prepared at different current densities (a) 20, (b) 10, (c) 1 mA/cm^2 at 30 °C, and (d) 20 mA/cm^2 at 65 °C.

solution of zinc nitrate-6-hydrate at near room temperature. Zn dominates the growth at higher current density. ZnO dominates the growth at higher deposition temperature. The PL peaks from ZnO and Zn are clearly observed and are a function of the deposition temperature and the current density. It is consistent with the results of XRD and FTIR examinations.

Acknowledgment. The authors gratefully acknowledge the support by the National Science Council of Republic of China under contract of NSC 94-2623-7-110-004.

References

(1) Özgür, Ü.; Alivov Ya., I.; Liu, C.; Teke, A.; Reshchikov, M. A.; Doğan, S.; Avrutin, V.; Cho, S.-J.; Morkoç, H *J. Appl. Phys.* **2005**, *98*, 041301.
(2) (a) Peulon, S.; Lincot, D. *Adv. Mater.* **1996**, *8*, 166. (b) Izaki, M.; Omi, T. *Appl. Phys. Lett.* **1996**, *68*, 2439.
(3) Xu, L.; Guo, Y.; Liao, Q.; Zhang, J.; Xu, D. *J. Phys. Chem. B* **2005**, *109*, 13519.
(4) Juárez, B. H.; López, C.; Alonso, C. *J. Phys. Chem.* **2004**, *108*, 16708.
(5) Chen, M. S.; Goodman, D. W. *Science* **2004**, *306*, 252.
(6) Lu, Y.; Yin, Y.; Li, Z.-Y.; Xia, Y. *Nano. Lett.* **2002**, *2*, 785.
(7) Lai, Y. K.; Shafi, V. P. M.; Ulman, A.; Loos, K.; Popovitz-Biro, R.; Lee, Y.; Vogt, T.; Estournés, C. *J. Am. Chem. Soc.* **2005**, *127*, 5730.
(8) Wang, J.-G.; Tian, M.-L.; Kumar, N.; Mallouk Th., E. *Nano Lett.* **2005**, *5*, 1247.
(9) Otani, S.; Katayama, J.; Umemoto, S.; Matsuoka, M. *J. Electrochem. Soc.* **2006**, *153*, C551.
(10) Könenkamp, R.; Word, R. C.; Godinez, M. *Nano Lett.* **2005**, *5*, 2005.
(11) Pauporté, Th.; Lincot, D. *Appl. Phys. Lett.* **1999**, *75*, 3817.
(12) Izaki, M.; Omi, T. *J. Electrochem. Soc.* **1997**, *144*, 1949.
(13) Izaki, M.; Omi, T. *J. Electrochem. Soc.* **1996**, *143*, L53.
(14) Paunovic M.; Schlesinger M. *Fundamentals of Electrochemical Deposition*, Wiley; New York, 1998, pp 108.
(15) Tong, Y.; Shao, M.; Qian, G.; Ni, Y. *Nanotechnology* **2005**, *16*, 2512.
(16) Watanabe, M.; Sakai, M.; Shibata, H.; Tampo, H.; Fons, P.; Iwata, K.; Yamada, A.; Matsubara, K.; Sakurai, K.; Ishizuka, S.; Niki, S.; Nakahara, K.; Takasu, H. *Appl. Phys. Lett.* **2005**, *86*, 221907.
(17) Cao, B.; Teng, X.; Heo, S. H.; Li, Y.; Cho, S. O.; Li, G.; Cai, W. *J. Phys. Chem. C* **2007**, *111*, 2470.
(18) Cao, B.; Cai, W.; Zeng, H.; Duan, G. *J. Appl. Phys.* **2006**, *99*, 073516.
(19) Li, G.-R.; Lu, X.-H.; Qu, D.-L.; Yao, C.-Z.; Zheng, F.-L; Bu, Q.; Dawa, C.-R.; Tong, Y.-X. *J. Phys. Chem. C* **2007**, *111*, 6678.
(20) Izaki, M.; Watase, S.; Takahashi, H. *Adv. Mater.* **2003**, *15*, 2000.
(21) Wong, E. M.; Searson, P. C. *Appl. Phys. Lett.* **1999**, *20*, 2939.
(22) Chen, Y.; Bagnall, D. M.; Koh, H.-j.; Park, K.-t.; Hiraga, K.; Zhu, Z; Yao, T. *J. Appl. Phys.* **1998**, *84*, 3912.
(23) Lee, J. K.; Nastasi, M.; Hamby, D. W.; Lucca, D. A. *Appl. Phys. Lett.* **2005**, *86*, 171102.
(24) Liu, X.; Wu, X.; Cao, H; Chang, R. P. H. *J. Appl. Phys.* **2004**, *95*, 3141.

CG060857T